Supporting Information

Achieving a High Loading of cathode in PVDF-based Solid-State Battery

Yang Liu[a,c], Xufei An [a,c], Ke Yang[a], Jiabin Ma[a], Jinshuo Mi[a] Danfeng Zhang[a], Xing Cheng[a], Yuhang Li[a], Yuetao Ma, Ming Liu[a,*], Feiyu Kang[a,b] and Yan-Bing He [a,*]

[a] *Shenzhen All-Solid-State Lithium Battery Electrolyte Engineering Research Center, Institute of Materials Research (IMR), Tsinghua Shenzhen International Graduate School, Shenzhen 518055, China.*

[b] *School of Materials Science and Engineering, Tsinghua University, Beijing 100084, China.*

[c] *These authors contributed equally to this work*

Correspondence to he.yanbing@sz.tsinghua.edu.cn, liuming@sz.tsinghua.edu.cn

Experimental Section

Materials. The commercial $LiNi_{0.8}Co_{0.1}Mn_{0.1}O_2$ (NCM811), polyvinylidene difluoride (PVDF5130, Mw=1,200,000, particle size: 100 μm, 99.5%), Super P (particle size: 40~50 nm, 99.5%), Al foil (thickness: 10 μm, 99.9%) , Coin cell components (CR2032, spacer: 15.8 ×1 mm, spring: 15.4×1.1 mm) and LiFSI ($LiF_2NO_4S_2$) were purchased from Guangdong Canrd New Energy Technology Co., Ltd. PVDF 761 (Mw= 600,000) came from Sigma Aldrich. N-methyl-2-pyrrolidone (NMP, AR) was purchased from Shanghai Aladdin Biochemical Technology Co., Ltd. Lithium foil (thickness: 450 μm, diameter:15.6 μm) and double side coated Cu foil (20 μm Li each side and the thickness of Cu is 10 μm, the whole thickness of Li anode is 50 μm) came from China Energy Lithium Co., Ltd.

Preparation of C@LATP NW. The C@LATP NW were synthesized via an electrospinning method and following an annealing process in argon atmosphere. In a typical procedure, 0.6 mmol $Al(NO_3)_3\cdot9H_2O$, 2.1 mmol $LiNO_3$, 0.8 mmol $Ti(OC_4H_9)_4$ and 4.5 mmol $C_6H_7O_3P$ were dissolved in 15 mL DMF by magnetic stirring at room temperature. Then, 0.86 g $C_6H_8O_7$ and 1.75 g PVP were added into the above solution and stirred for 12 h to obtain a homogeneous stable spinning sol, which was then electrospun into C@LATP NW precursors under the electrospinning voltage of -1~20 kV and pumping rate of 1.5 mL h^{-1}. The precursors were calcined at 800 °C in argon atmosphere for 6 h with the heating rate of 5 °C min^{-1} to obtain C@LATP NW.

Preparation of LATP NW. The LATP NW were synthesized via an electrospinning method and following an annealing process in argon atmosphere. In a typical procedure, 0.6 mmol $Al(NO_3)_3\cdot9H_2O$, 2.1 mmol $LiNO_3$, 0.8 mmol $Ti(OC_4H_9)_4$ and 4.5 mmol $C_6H_7O_3P$ were dissolved in 15 mL DMF by magnetic stirring at room temperature. Then, 0.86 g $C_6H_8O_7$ and 1.75 g PVP were added into the above solution and stirred for 12 h to obtain a homogeneous stable spinning sol, which was then electrospun into LATP NW precursors under the electrospinning voltage of -1~20 kV and pumping rate of 1.5 mL h^{-1}. The precursors were calcined at 800 °C in air atmosphere for 6 h with the heating rate of 5 °C min^{-1} to obtain LATP NW.

Preparation of PVDF-LLZTO electrolytes. PVDF powders and LLZTO particles were dried at 60 °C for 12 h before use to remove trapped water. Self-standing PVDF-LLZTO electrolytes were prepared by solution casting method. The weight percentage of LLZTO in the mass of PVDF was 25%. In a typical experiment, 400 mg PVDF, 267 mg LiFSI were dissolved in 15 mL DMF solvent

and stirred at 40 °C for 6 h to obtain a homogeneous solution, then the LLZTO were added into the solution. After that, the homogenized mixture was poured into culture dish mold. Finally, the solid-state electrolytes were obtained by drying for 24 h at 55 °C under air-blower oven and stored in glovebox for 10 h before use.

Preparation of the PCL-NCM composite cathode and full cell. The PCL-NCM composite cathode was prepared through a traditional slurry mixing process and coated on an aluminum foil. The PCL-NCM cathode slurry was prepared by mixing NCM811 particles, PVDF, Super P and C@LATP NW with the weight radio of 8 : 1 : (1-x) : x. C@LATP NW with different weight ratios of 0% (P-NCM), 1%, 3%, 5% and 7% were added to the composite cathode slurry (PCL-NCM). Then, the cathode slurry was cast on an Al foil and dried at 60 °C for 12 h. The PL-NCM cathode with LATP NW was prepared in the same way as PCL-NCM. CR2032 coin cells were assembled using Li foil as the anode, P-NCM, PL-NCM or PCL-NCM as the cathode, and PVDF-LLZTO as the electrolyte in a glove box. During the fabrication process, pressure such of 700 kg has been applied to the coin cell for holding 5 s. The thickness of lithium foil is 450 μm and the diameter is 15.6 mm. The diameter of cathode is 12 mm, and the thickness of PVDF-LLZTO electrolyte is 70 μm. In the coin cell, 2 spacers and a spring was used in the cell. In a typical experiment, cathodes were pressed to half of their initial thickness before battery assembly.

Assembly of Solid-state NCM811/Li pouch cells. A pouch cell was fabricated with NCM cathode with C@LATP·NW (PCL-NCM), lithium metal and PVDF-LLZTO electrolyte. Please note that the cathode and anode each has a metal lug (Al for cathode and Cu for anode with 1 cm ×1 cm dimension). The dimensions of cathode, electrolyte and lithium anode are shown in **Fig. S25**a-c. To be specific, the cathode, electrolyte and lithium anode cathode are stacked on top of each other in sequence (**Fig. S25**d) and finally be sealed in the Al plastic film package. During the fabrication and formation process, pressure such of 700 kg has been applied to the pouch cell to ensure the excellent contact between PVDF-LiFSI-LLZTO electrolyte and electrodes. We assembled in a dry room whose dew point is -50 °C.

Materials Characterization. The X-ray diffraction (XRD) measurements of the samples were characterized on a Bruker D8 Advance with Cu-Kα radiation. The operando XRD tests during charging and discharging rate of 0.1C were performed at 25 °C and diffraction patterns were collected every 8 min. The morphology was analyzed by scanning electron microscope (SEM, HITACH S4800) with energy dispersive spectroscopy. The structure was analyzed by a field emission transmission electron

microscope (FE-TEM, FEI Tecnai F30). X-ray photoelectron spectroscopy (XPS) measurement was collected on a PHI 5000 VersaProbe II instrument. The Fourier transform infrared (FTIR) spectra was executed by VERTEX 70 spectrometer in an attenuated total reflection (ATR) mode. The microscopic Fourier transform infrared spectroscopy (FTIR) was performed to evaluate the diffusion of $[Li(DMF)_x]^+$ at different cross-sectional depths of high-loading cathode. The AFM-nano-infrared examinations were performed with a Bruker Anasys nanoIR2-fs instrument. The Raman spectra was obtained by HORIBA LabRAM HR800. Thermogravametric analysis (TGA) was performed using a Netzsch STA 449F3 thermal analyzer from room temperature to 1000 °C in air atmosphere. The specific surface area (BET) of each sample were calculated on a Micromeritics-ASAP 2020 analyzer from nitrogen adsorption.

Electrochemical measurements. The ionic conductivities of PVDF-LLZTO were measured by electrochemical impedance spectroscopy (EIS) from 7 MHz to 0.1 Hz with a 20 mV AC oscillation on a VMP3 multichannel electrochemical station (Bio Logic Science Instruments, France). The cells were assembled by a small piece of PVDF-LLZTO slice sandwiched between two stainless-steel (SS-SS) blocking electrodes. The ionic conductivities (σ) were calculated following equation S1:

$$\sigma = \frac{L}{RS}$$

(S1)

where L is the thickness of electrolytes, R is obtained by EIS measurement with electrolytes sandwiched between two stainless plates of steel, and S is the area of stainless steel.

The Li$^+$ apparent diffusion coefficient of PCL-NCM and P-NCM can be evaluated through I$_p$ and $\upsilon^{1/2}$ at various scan rates from the following Randles-Sevcik equation (equation S2):

$$I_p = 0.4463n^{3/2}F^{3/2}AR^{-1/2}T^{-1/2}D^{1/2}C\upsilon^{1/2}$$

(S2)

where Ip (A) is the peak current, n is the charge transfer number per molecule during the redox reaction, F is the Faraday constant (96485 C mol^{-1}), C (mol cm^{-3}) is the concentration of Li$^+$, A (cm^2) is the electrode surface area, R is the gas constant (8.314 J mol^{-1} K^{-1}), T (K) is the absolute temperature, D (cm^2 s^{-1}) is the apparent Li$^+$ diffusion coefficient from CV measurements, and υ (V s^{-1}) is the scanning rate.

The Li$^+$ diffusion coefficients of PCL-NCM and P-NCM were determined by the GITT using the Land battery testing system (LAND CT2001A). The cells were charged/discharged repeatedly at 0.1C for 1 h, and stayed for 6 h at an open circuit. Assuming that the Li$^+$ transportation in the electrode

obeys Fick's second law and a steady voltage can be obtained after relaxation process, the apparent Li^+ chemical diffusion coefficients (D_{Li+}) can be determined by equation S3:

$$D_{L_i^+} = \frac{4}{\pi}\left(I_0\frac{V_m}{FS}\right)^2(\frac{dE/dx}{dE/d\tau^{1/2}})^2, \tau \ll \frac{L^2}{D_{Li^+}}$$

(S3)

where D_{Li}^+ (cm^2 s^{-1}) is the Li^+ apparent chemical diffusion coefficient, V_m (cm^3 mol^{-1}) is the molar volume of NCM, I_0 (A) is the pulse current, F is the Faraday constant (96485 C mol^{-1}), S (cm^2) is the electrode surface area, and L (cm) is the diffusion length. dE/dx (V) is the change of the open circuit E corresponds to x, and $dE/d\tau^{1/2}$ (V $s^{-1/2}$) means that the charge voltage differentiates the square root of time ($\tau^{1/2}$) during the charge process.

The NCM811/Li full cells were assembled for the cyclic voltammetry (CV) measurements in the voltage range of 2.8~4.3 V using a VMP3 multichannel electrochemical station. Galvanostatic charge/discharge tests of cells were performed on a battery test system (LAND CT2001A) and Neware battery cycler (CT-4008T-5V10mA-164, Shenzhen, China) with a voltage range from 2.8 to 4.3 V at room temperature. The cycled cells were transferred into a glovebox and dissembled for further examination. The NCM811 cathode and lithium metal anode were transferred into a chamber with a sealed Ar-filled vessel for SEM and XPS examination.

DFT calculations. The highest occupied molecular orbital and lowest unoccupied molecular orbital (HOMO and LUMO) energy of DMF and $[Li(DMF)_3]^+$ was calculated by quantum-chemical calculations (based on density functional theory, B3LYP/6-311G (d, p)).

Supporting Tables

Table S1 BET data of C@LATP NW, LATP NW and NCM811

Physical quantities	Numerical			Unit
	C@LATP NW	LATP NW	NCM811	
V_m	66.542	1.834	0.1848	[cm^3(STP) g^{-1}]
$a_{s,BET}$	289.62	7.9825	0.80432	[m^2 g^{-1}]
C	82.12	275.04	92.657	-
Total pore volume(p/p_0=0.360)	0.2983	0.031056	0.000419	[cm^3 g^{-1}]
Mean pore diameter	4.1196	15.562	2.085	[nm]

Supporting Figures
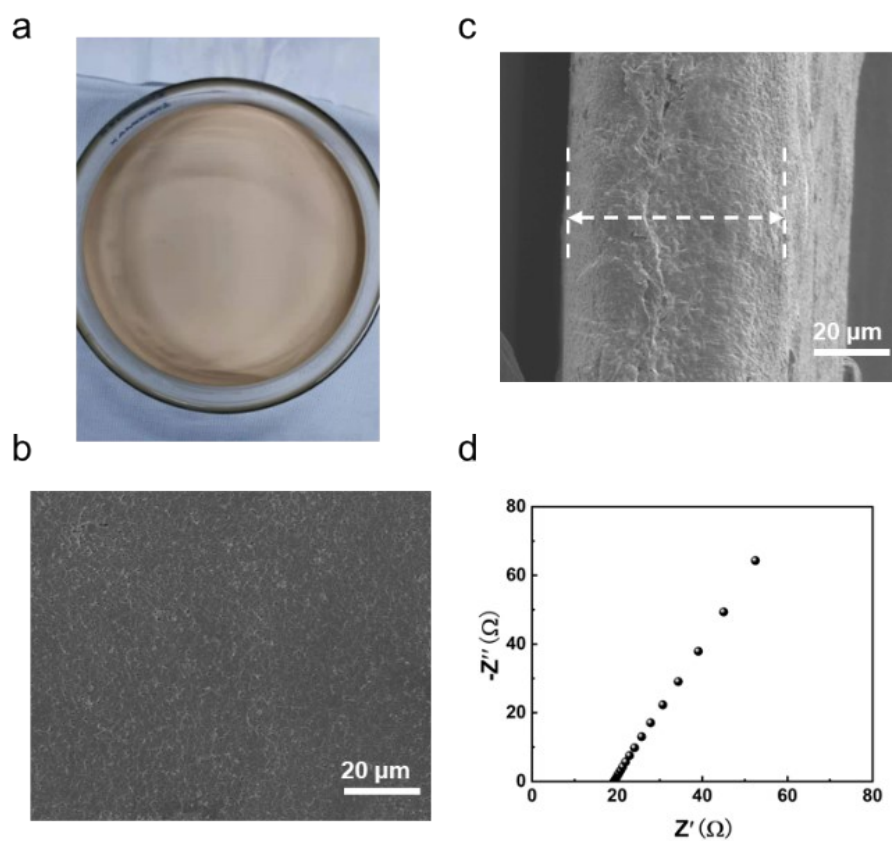
Fig. S1 (a) Optical image of PVDF-LLZTO SPEs. (b) Surface SEM images and (c) cross-sectional SEM images of PVDF-LLZTO SPEs. (d) EIS of PVDF-LLZTO SPEs.
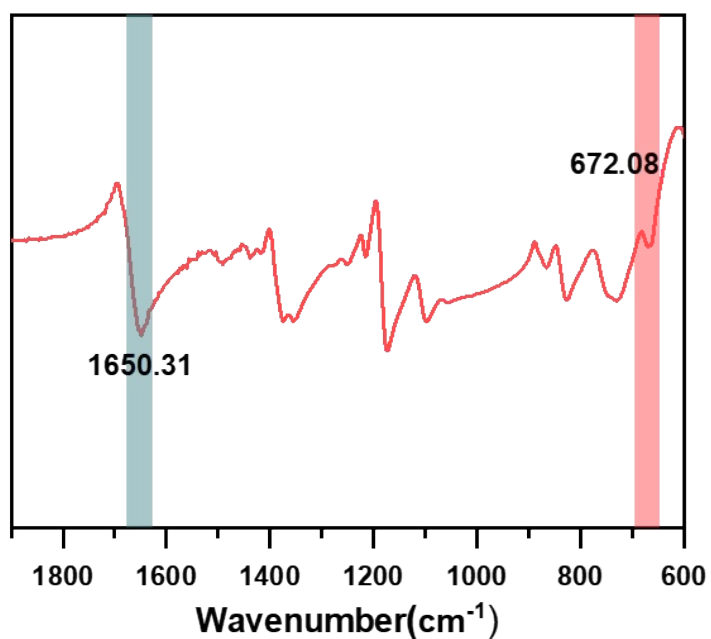
**Fig. S2** FTIR spectra of NCM811 cathode.

a

b
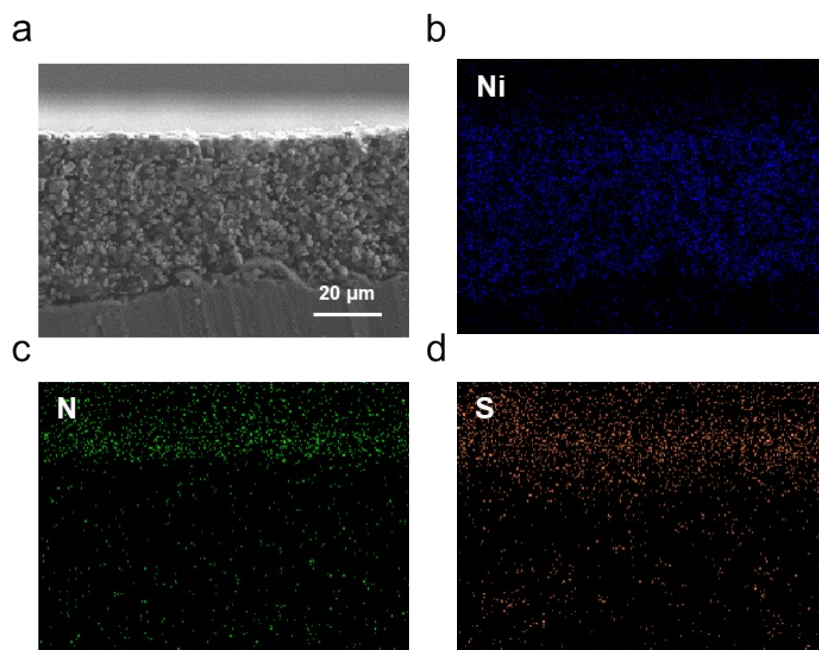
Fig. S3 (a) Cross section SEM image of the NCM811 cathode of an uncycled NCM811/PVDF-LLZTO/Li solid state battery after standing for 12 h and its EDS mapping of the (b) Ni, (c) N and (d) S elements.

a

b

c
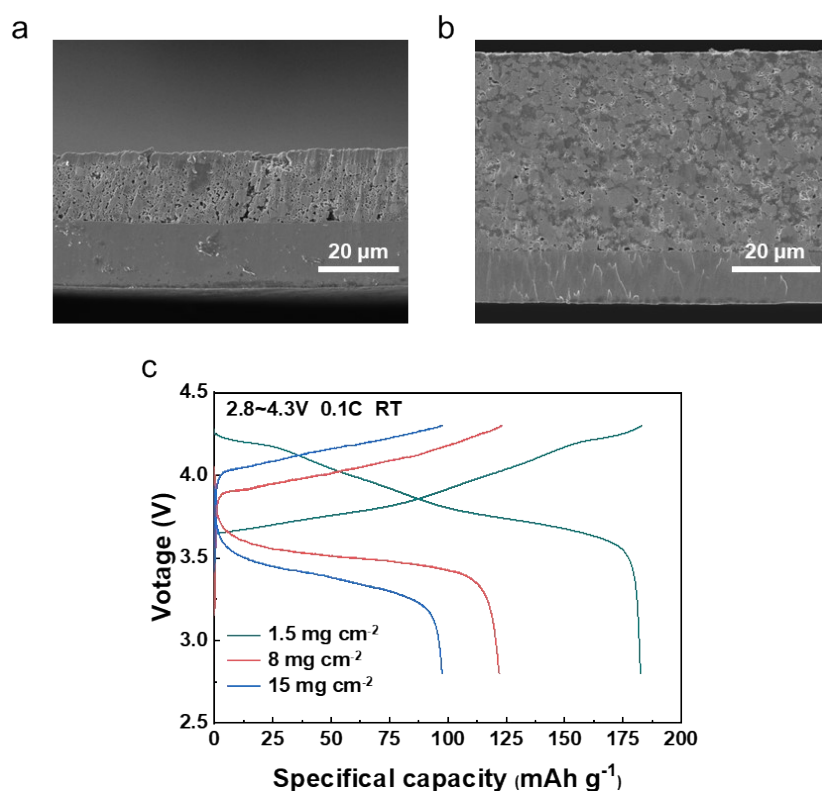
Fig. S4 SEM image of a cross-section of (a) the cathode with 1.5 mg cm^{-2} NCM811 loading and (b) the cathode with 15 mg cm^{-2} NCM811 loading. (c) Charge/discharge curves of PVDF based SSLMBs with different NCM811 loadings of 1.5 mg cm^{-2}, 8 mg cm^{-2} and 15 mg cm^{-2} at 0.1C at RT.
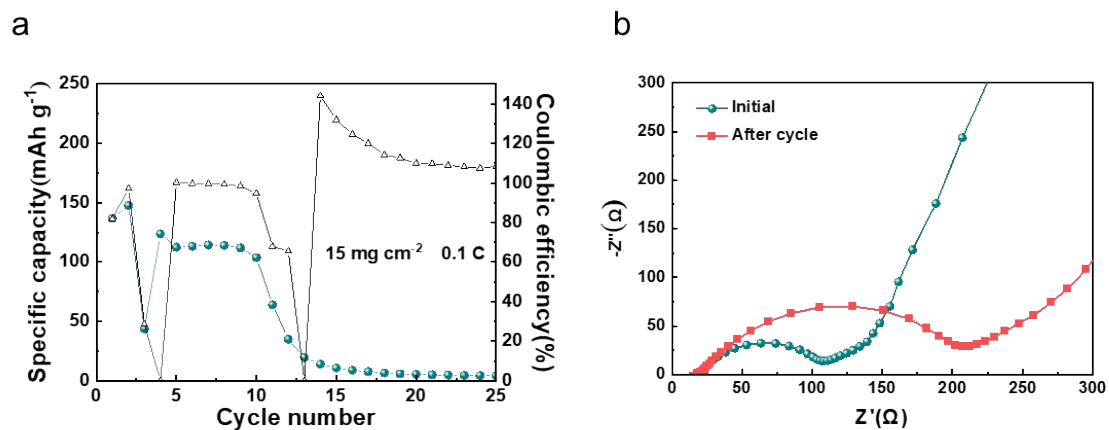
Fig. S5 (a) Cycling stability of the NCM811/PVDF-LLZTO/Li solid-state batteries with NCM811 loading of 15 mg cm^{-2} at 0.1 C and (b) Electrochemical impedance spectroscopy of NCM811/PVDF-LLZTO/Li full cells before and after the cycle.
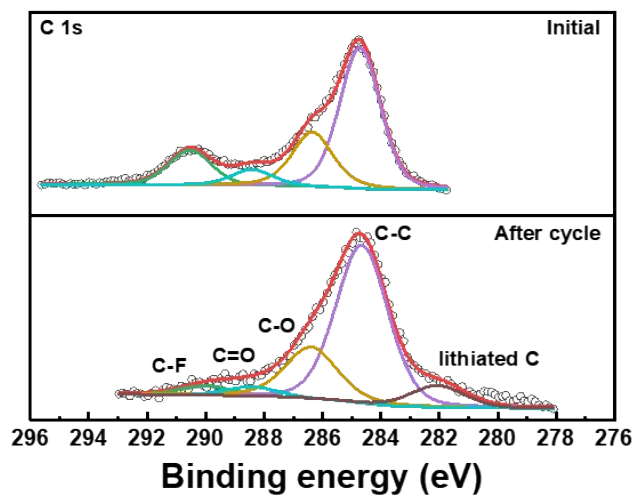
Fig. S6 XPS spectra for C 1s of cycled NCM811 cathode.
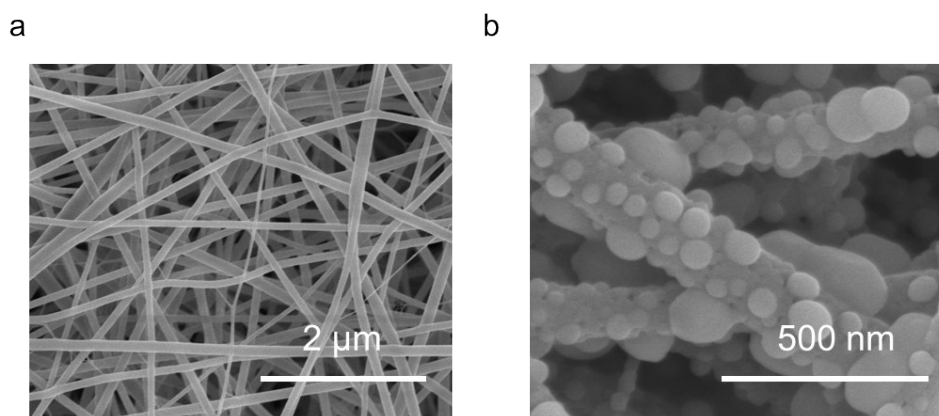
Fig. S7 SEM images of (a) C@LATP NW precursor and (b) C@LATP NW.
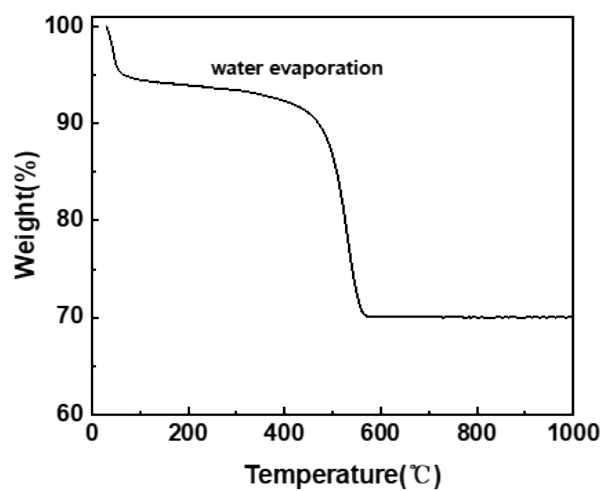
Fig. S8 The thermogravimetric analysis (TGA) test of C@LATP NW.
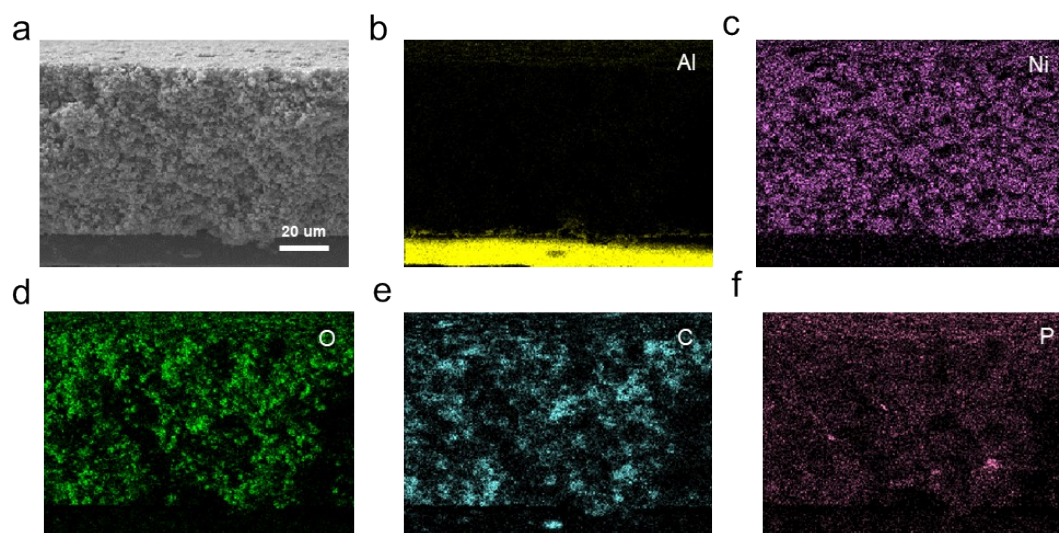
Fig. S9 (a) Cross section SEM image of the PCL-NCM with 3 wt.% C@LATP NW and its EDS mapping of the (b) Al, (c) Ni, (d) O, (e) C and (f) P elements.
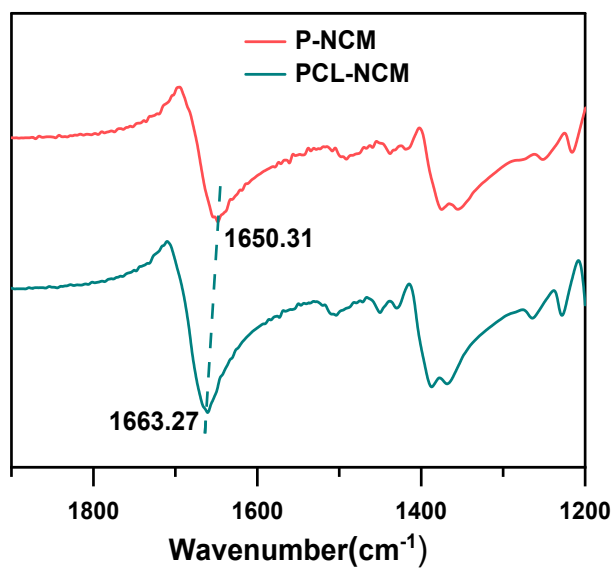
Fig. S10 FTIR spectra of P-NCM and PCL-NCM cathode.
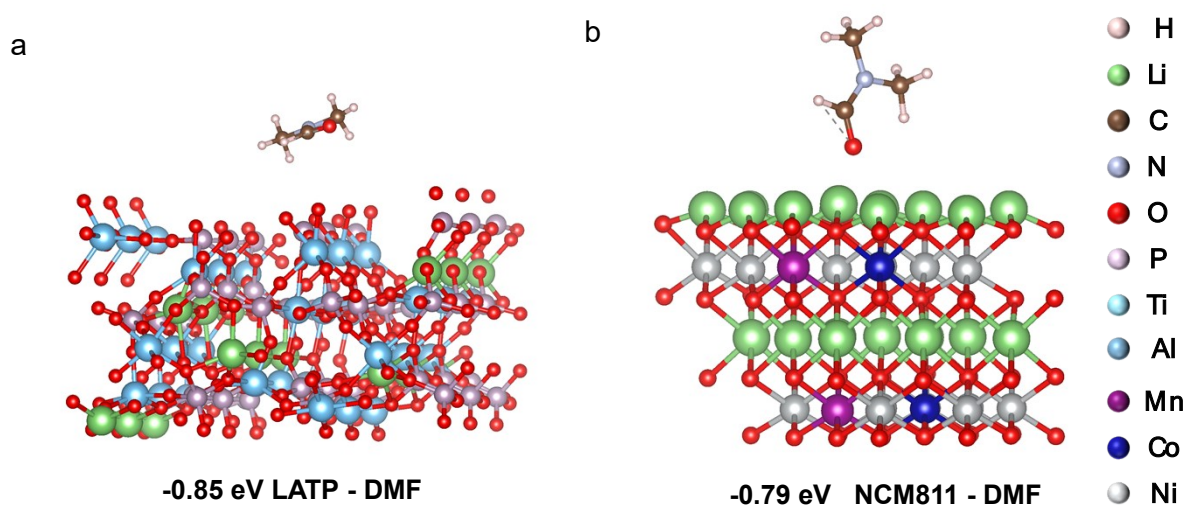
Fig. S11 DFT calculation results of adsorption energy of (a) LATP NW with DMF and (b) NCM811 with DMF.
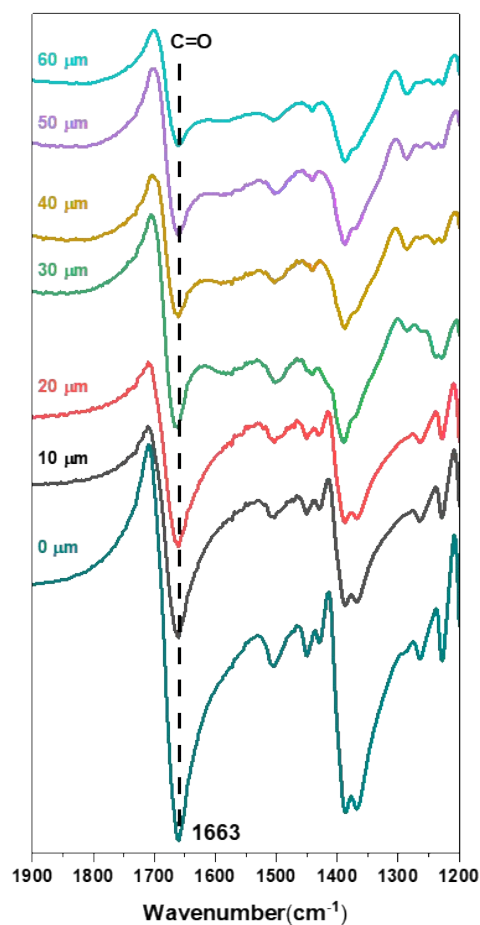
Fig. S12 FTIR spectra of PCL-NCM at different depth.
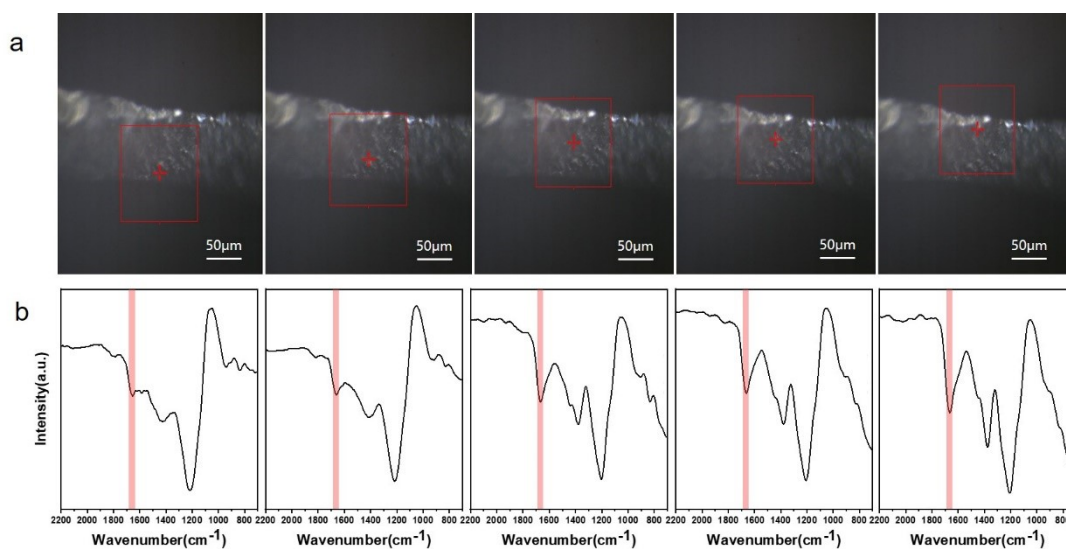
Fig. S13 a) The microscopic images of PCL-NCM cathode and b) FTIR spectra of cathode at different cross-sectional depths.
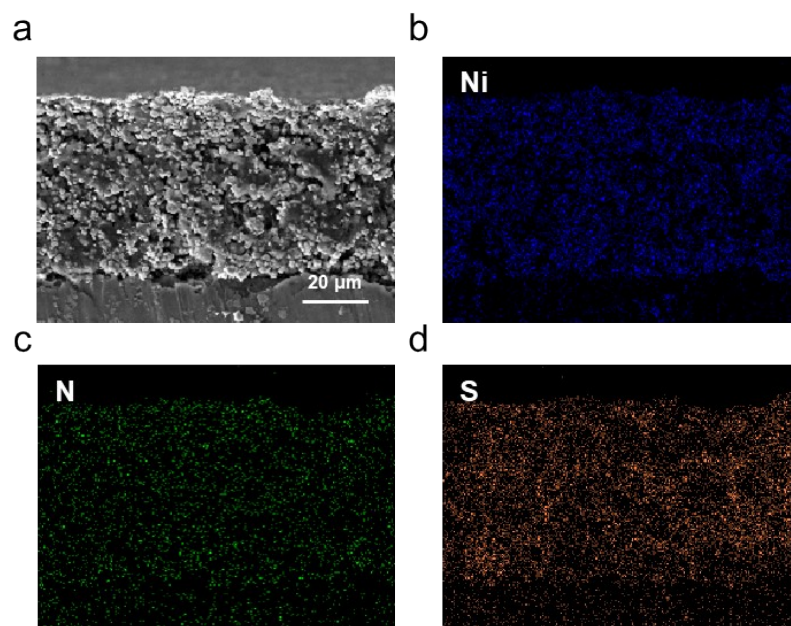
Fig. S14 (a) Cross section SEM image of the PCL-NCM cathode of an uncycled PCL-NCM/PVDF-LLZTO/Li solid-state cell after standing for 12 h and its EDS mapping of the (b) Ni, (c) N and (d) S elements.
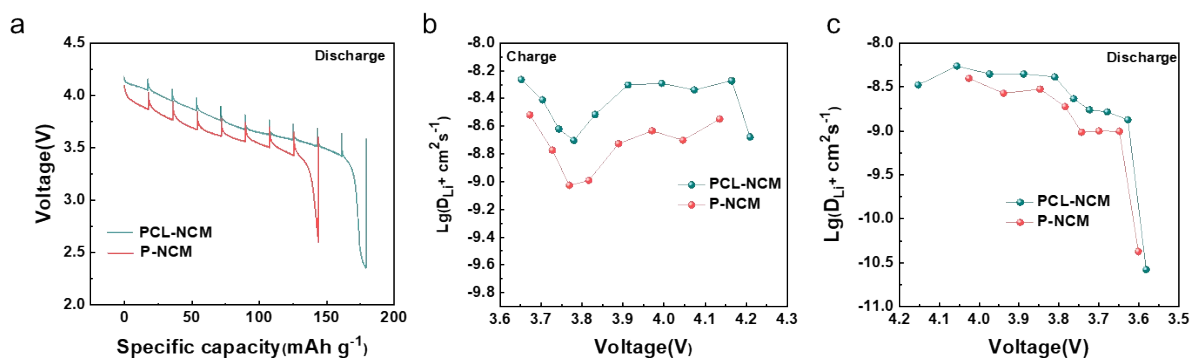
Fig. S15 (a) GITT plots of the PCL-NCM and P-NCM cathode in discharge process and the Li-ion diffusion coefficients in (b) charge and (c) discharge process measured by GITT.
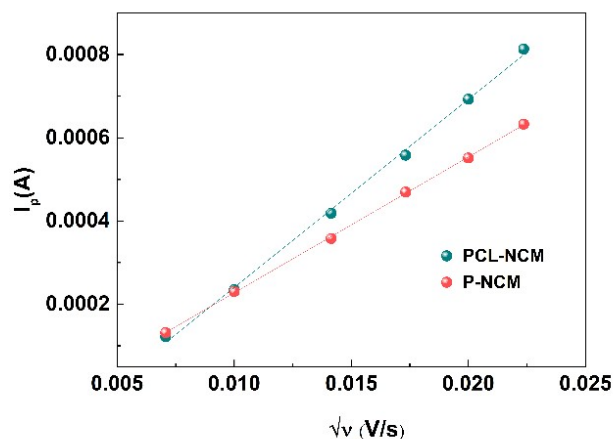
Fig. S16 The plots of peak current (I_p) as a function of the square root of the scan rate $v^{1/2}$ for PCL-NCM and P-NCM.
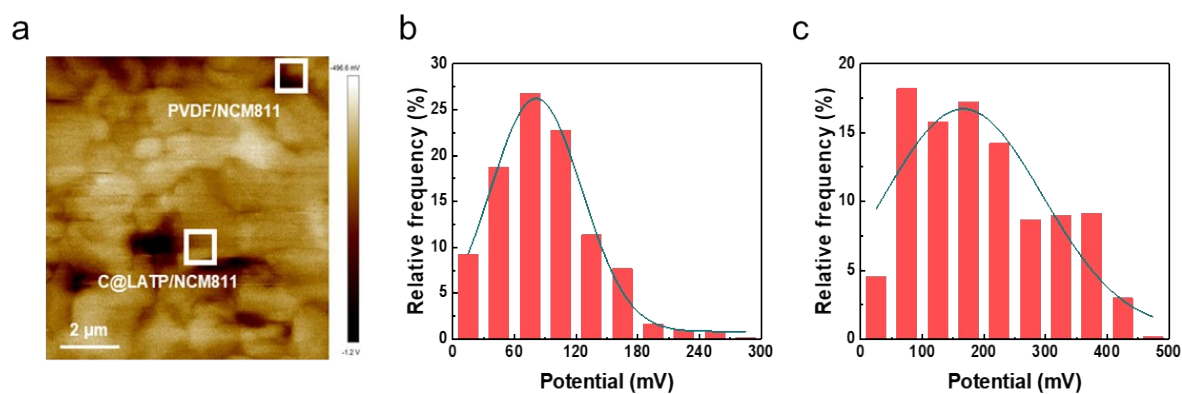
Fig. S17 (a) Kelvin probe force microscopy interfacial potential images of the PCL-NCM. Gauss statistic distribution histograms of the interfacial potential for the (b) C@LATP-NCM811 and (c) PVDF-NCM811.
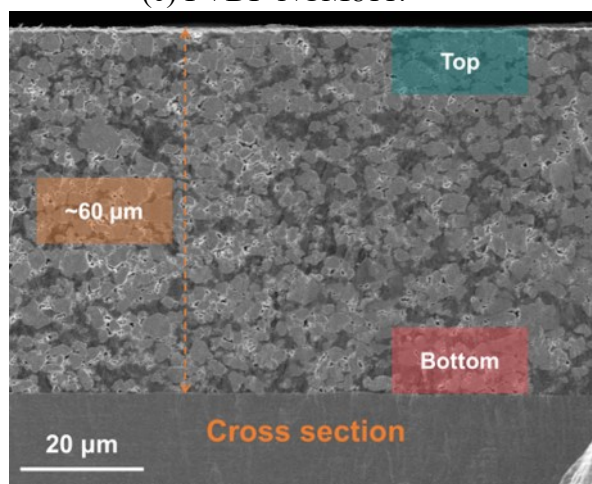
Fig. S18 SEM image of cathode section.
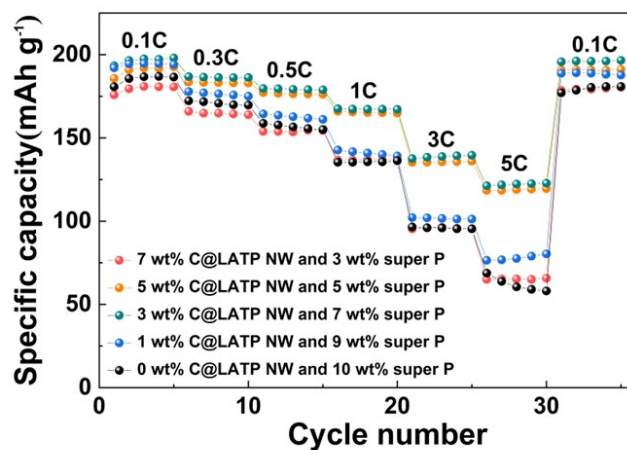
Fig. S19 Rate performance of PCL-NCM/PVDF-LLZTO/Li full cell with different weight ratios of C@LATP NW and Super P.
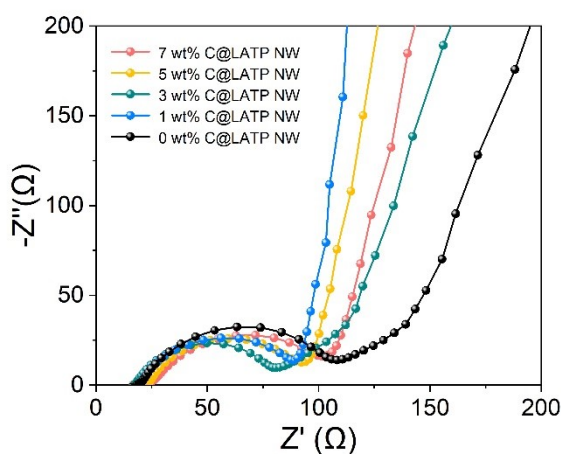
Fig. S20 Electrochemical impedance spectroscopy of the PCL-NCM/PVDF-LLZTO/Li full cells with different weight ratios of C@LATP NW at 50% state of charge.
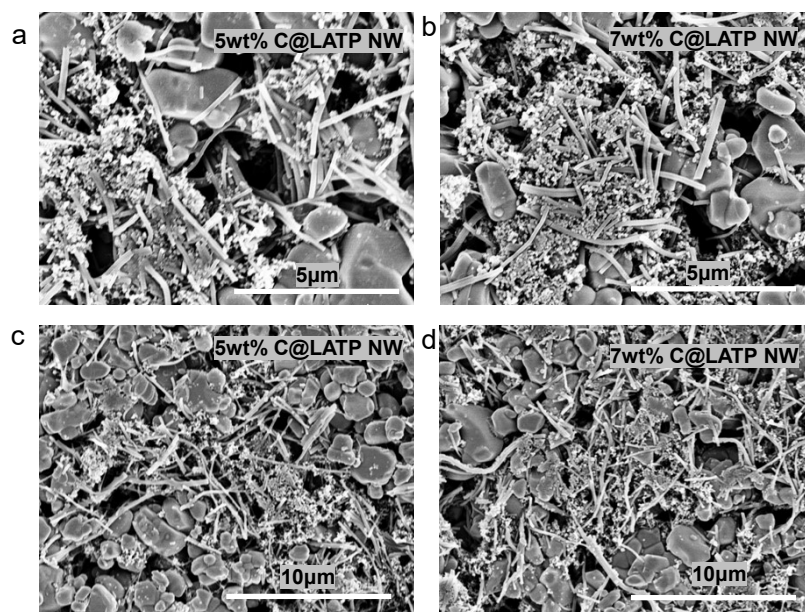
Fig. S21 SEM images of a) and c) PCL-NCM cathode with 5% C@LATP NW at different magnifications; b) and d) PCL-NCM cathode with 7% C@LATP NW at different magnifications.
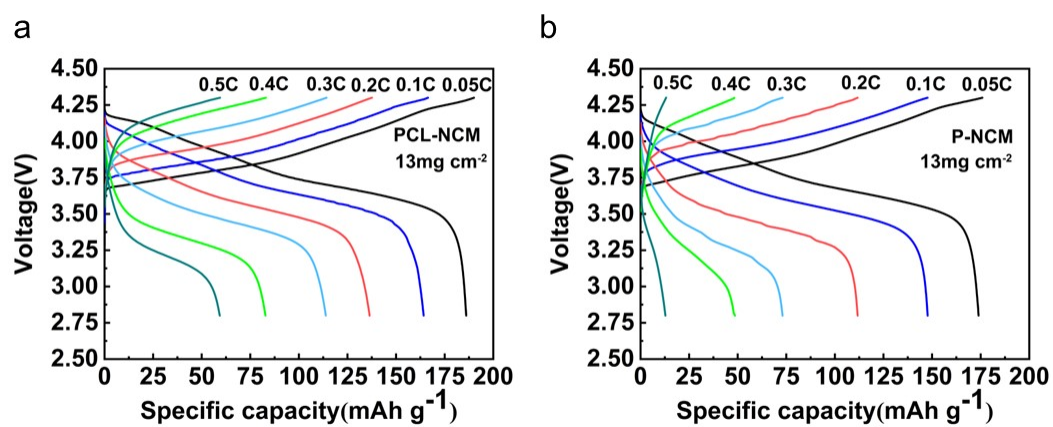
Fig. S22 Charge/Discharge curves of (a) PCL-NCM/PVDF-LLZTO/Li and (b) P-NCM/PVDF-LLZTO/Li full cell at 0.05 C, 0.1 C, 0.2 C, 0.3 C, 0.4C and 0.5 C.
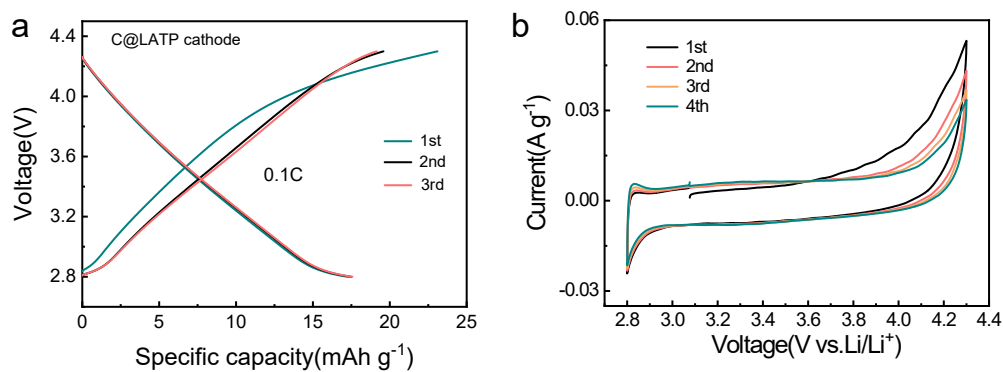
Fig. S23 a) Charge/discharge curves of C@LATP NW/Li cell; b) Cyclic voltammetry measurements of C@LATP NW/Li cell.
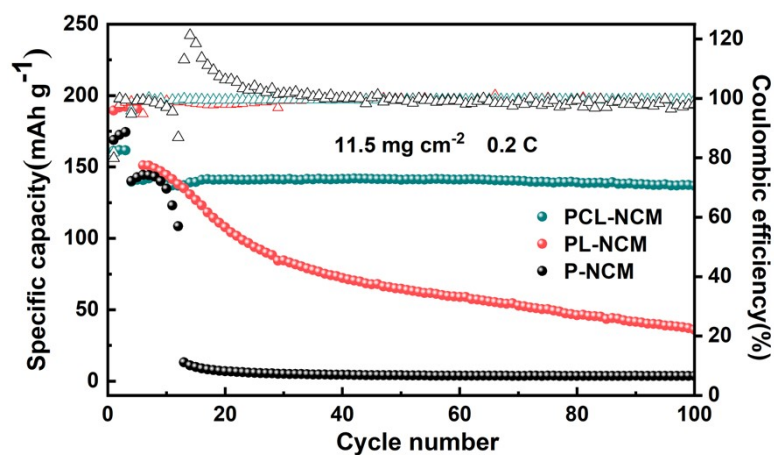
Fig. S24 Cycling stability of the NCM811/Li solid-state batteries with NCM811 loadings of 11.5 mg cm^{-2} at 0.2 C.
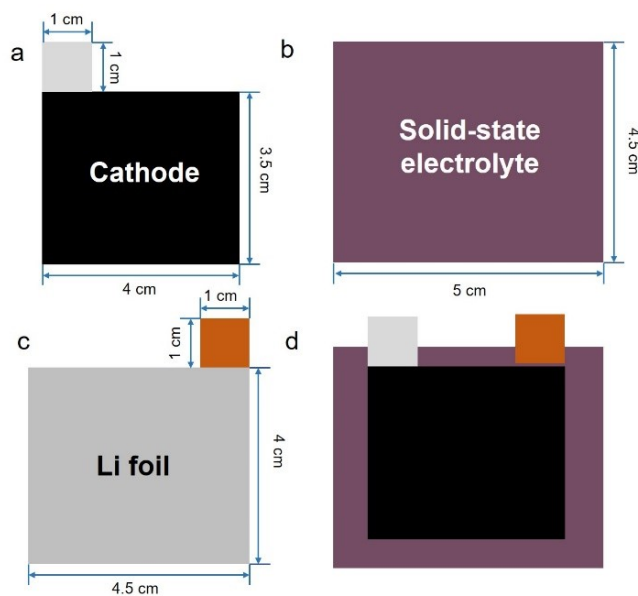
Fig. 25 Schematic diagram of each component of a pouch cell: (a) cathode, (b) solid-state electrolyte, (c) lithium anode, (d) diagram of stack sequence and an integrated pouch cell sealed in Al plastic film package.
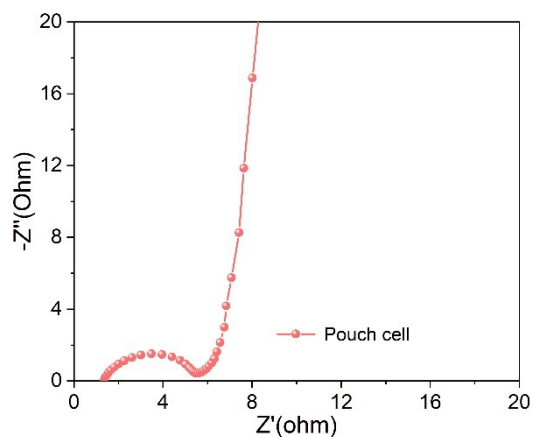
Fig. S26 Nyquist impedance spectra of the Li/PVDF-LLZTO/PCL-NCM pouch cell.
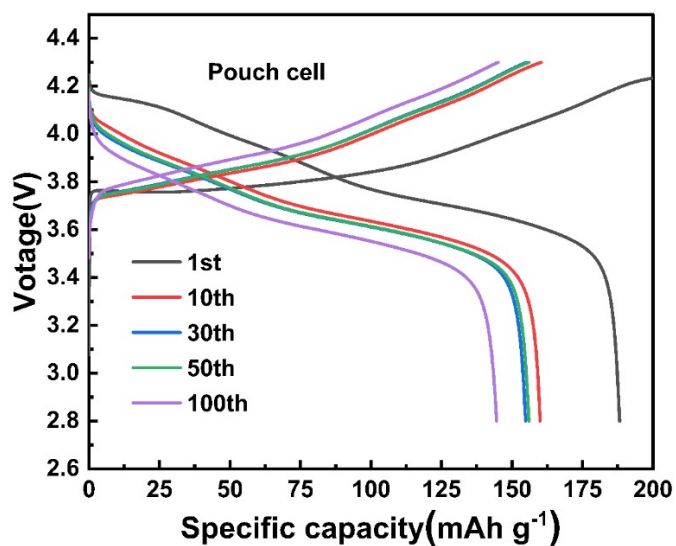
Fig. S27 Charge/discharge curves of PCL-NCM/PVDF-LLZTO/Li pouch cell with NCM811 loadings of 8.6 mg cm^{-2} at 0.1C.
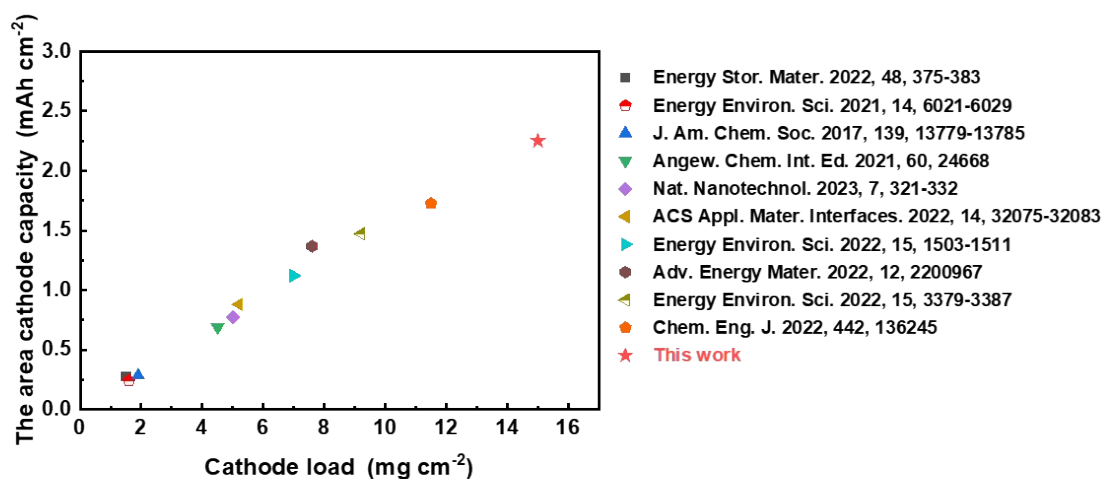

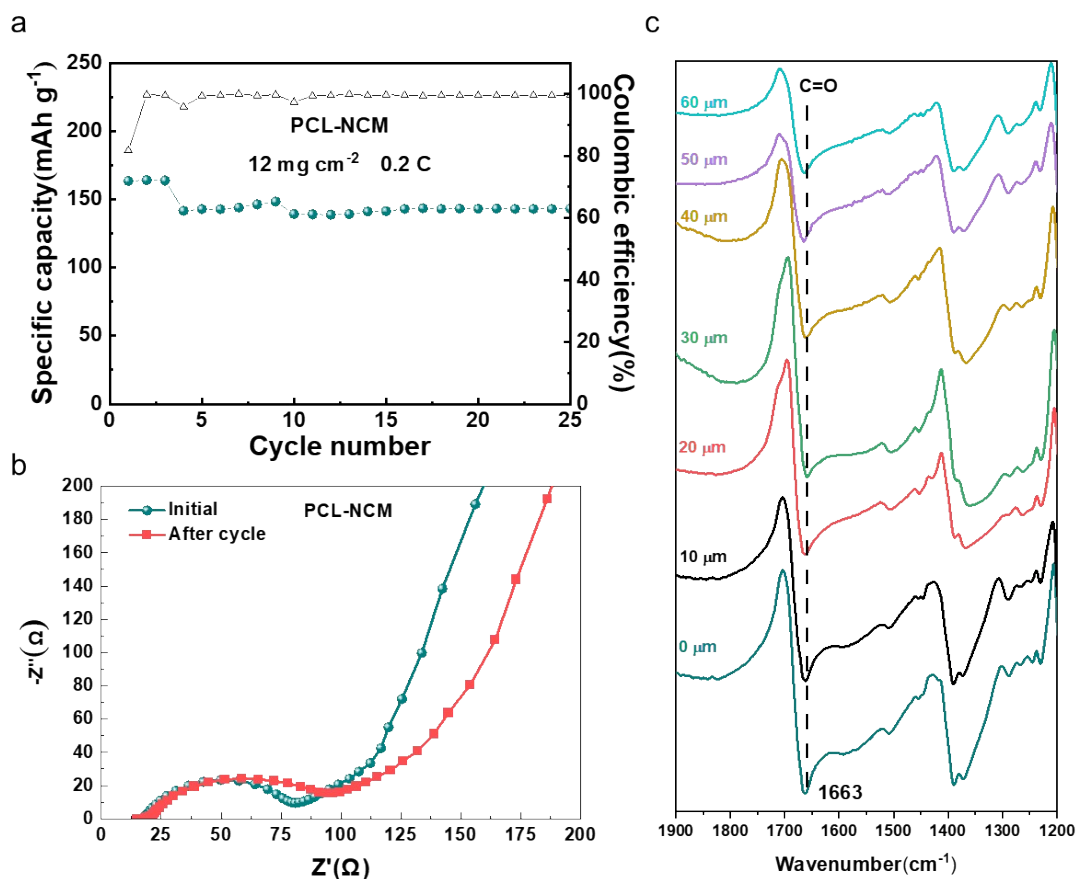**Fig. S28** Performance comparison of reported PVDF-based SSLMBs with high loading cathode.

Fig. S29 (a) Cycling stability of the PCL-NCM/PVDF-LLZTO/Li solid-state batteries with NCM811 loadings of 12 mg cm^{-2} at 0.2 C and (b) Electrochemical impedance spectroscopy of PCL-NCM/PVDF-LLZTO/Li full cells before and after the cycle. (c) FTIR spectra of cycled PCL-NCM at different depth.
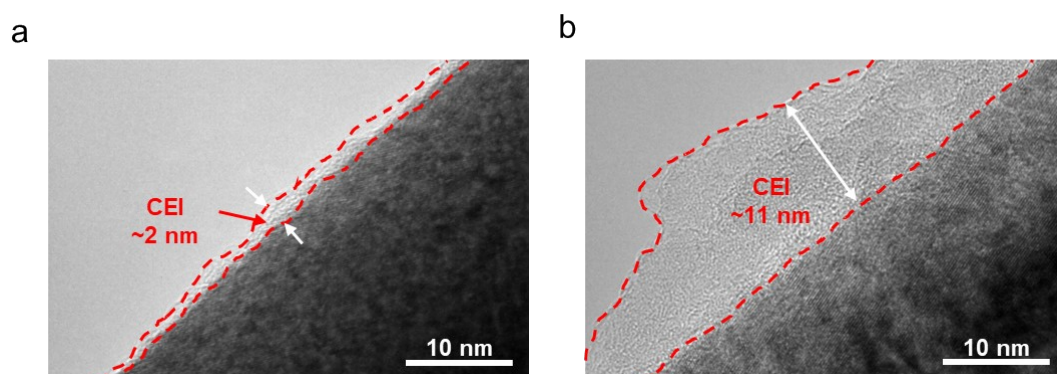

Fig. S30 TEM images of the cycled (a) PCL-NCM and (b) P-NCM.

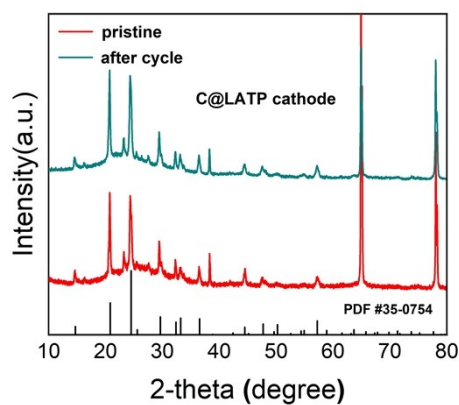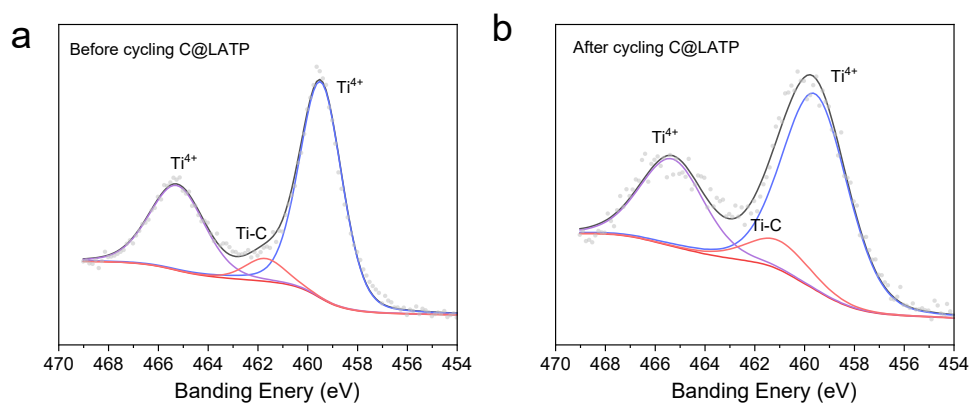**Fig. S31** XRD spectra of the C@LATP NW before and after cycling.

Fig. S32 XRS spectra of the C@LATP NW before and after cycling.